Robotica (2015) volume 33, pp. 1909–1925. © Cambridge University Press 2014
doi:10.1017/S0263574714001118

Dynamic characteristics of a 3-RPR planar parallel manipulator with flexible intermediate links

Amirhossein Eshaghiyeh Firoozabadi, Saeed Ebrahimi* and Ghasem Amirian

Department of Mechanical Engineering, Yazd University, Yazd, Iran

(Accepted April 12, 2014. First published online: May 13, 2014)

SUMMARY

This paper presents the dynamic modeling of a 3-RPR planar parallel manipulator with three flexible intermediate links in order to investigate the effects of the intermediate links flexibility on the undesired vibrations of the end-effector. For this purpose, the intermediate links are modeled as Euler–Bernoulli beams with two types of fixed-pinned and fixed-free boundary conditions based on the assumed mode method (AMM). The equations of motion of the 3-RPR manipulator are formulated using the augmented Lagrange multipliers method in the form of differential algebraic equations (DAEs) by incorporating the elastic and rigid coordinates in the set of generalized coordinates. After defining the initial conditions and imposing external forces to the manipulator, the equations are then solved numerically using the Modified Extended Backward-Differentiation Formula Implicit (MEBDFI) approach. Comparison of the simulation results for two different boundary conditions shows clearly the effects of flexibility of the intermediate links on the vibration of the end-effector trajectory. Results of this work can be used for the dynamic modeling of other manipulators or to design a controller for reducing the undesired vibrations.

KEYWORDS: Flexible manipulators; Parallel manipulators; Assumed mode method; Euler–Bernoulli beam.

1. Introduction

Now-a-days, parallel manipulators constitute an important part of industry, and their applications are increasing due to their speed and accuracy compared with serial manipulators. Therefore, many researches are devoted to this topic and seek to identify causes of deviation of the end-effector from its desired trajectory, reducing the amount of deviation, and optimizing and controlling manipulators. In industrial manipulators, the link and joint flexibility are two important sources of deviation from a desired trajectory. To verify and increase the accuracy of these manipulators, the structural flexibility of their links has to be considered and modeled in an effective and natural way. This is an important issue because transverse vibrations of the links as a result of the flexibility lead to deviation from a desired trajectory of the end-effector. Compared with serial manipulators, limited studies report the dynamic modeling of parallel manipulators with structural flexibility. These manipulators have closed loop geometry and consequently, their system equations of motion include the kinematic constraint equations. A detailed survey of the literature related to the dynamic analysis of flexible robotic manipulators has been carried out in ref. [1] including both link and joint flexibility.

Parallel manipulators typically consist of several closed chains and a moving platform. According to the arrangement of their joints in a chain, these mechanisms are classified as PRR, RPR, RRR, PRP, PRS, etc., where P denotes a prismatic joint, R denotes a revolute joint, and S denotes a spherical joint. The preliminary studies on this subject were dealing with the kinematic and dynamic analysis of rigid parallel manipulators. Due to the increasing demand of constructing parallel manipulators with high level of precision, the dynamic modeling of manipulators with flexible intermediate links has become

* Corresponding author. E-mail: ebrahimi@yazd.ac.ir

an interesting topic. In this context, mainly two approaches are used: finite element method (FEM) and assumed mode method (AMM). Theodore and Ghosal[2] compared FEM and AMM for modeling the link flexibility of manipulators. They showed that mathematical operations required for the inertia matrix computation in the FEM are fewer compared to the AMM formulation. However, due to the higher number of state space equations in FEM, the numerical simulation may be computationally more expensive.

Among the earliest works for considering the flexibility of parallel manipulators, the work of Lee and Geng[3] can be mentioned in which they developed the dynamic modeling of a flexible Stewart manipulator. With the consideration of link flexibility, Giovagnoni[4] presented a general approach for the dynamic analysis of flexible closed-chain manipulators using the principle of virtual work. Fattah[5] used FEM for discretization of the flexible links of a 3-DOF (degree of freedom) parallel manipulator. The equations of motion of the uncoupled links were derived based on the Euler–Lagrange formulation. Kang and Mills[6] presented a procedure for flexibility modeling in a flexible parallel manipulator, which thereafter became the basis for several researches. Using the Lagrange multipliers method, they developed the fully coupled equations of motion of a 3-PRR planar parallel manipulator by considering structural flexibility of the intermediate links. These links were modeled as Euler–Bernoulli beams with pinned-free boundary conditions based on the AMM. Wang and Mills[7] performed an experimental modal analysis of flexible links of a 3-PRR manipulator. They studied the boundary conditions which verify the experimental results. A dynamic model for a 3-PRR planar parallel manipulator with flexible links was developed based on the FEM in refs. [8] and [9]. Zhou *et al.* derived equations of motion of a 3-PRS manipulator with flexible links and joints for vibration analysis using the FEM.[10] They combined the finite element models of the link and the joint virtual spring models. All the links were modeled by finite elements in which triangular membranes were combined with bending plates for the moving platform and spatial beams for the legs. Using the same procedure, Zhang *et al.*[11,12] developed the equations of motion of a 3-PRR parallel manipulator by modeling the intermediate links with pinned-pinned boundary conditions based on the Lagrange multiplier method. They studied the effect of elastic deformations on rigid body motions and coupling effect between flexible links. In ref. [12] the effect of concentrated rotational inertia at both ends of the intermediate links was included in this model. Experimental modal tests were performed to validate the theoretical model through comparison and analysis of modal characteristics of the flexible manipulator system. They also improved that procedure by considering longitudinal flexibility of the manipulator links to derive equations.[13] Open-loop simulation without joint motion controls and closed-loop simulation with joint motion were performed to investigate the effect of elastic motions on rigid body motions and coupling effect between flexible links. In addition, dynamic behavior of the same manipulator including the effect of axial forces on the lateral deformations was investigated.[14] Finally, they presented multi-mode vibration control and analysis of moving platform position errors of that manipulator using piezoelectric transducers (PZTs).[15]

Dynamic modeling and vibration control of a 3-PRR planar parallel manipulator with flexible linkages were considered in ref. [16]. The AMM is adopted with the pinned-pinned boundary conditions to include the structural flexibility. Therein, an active damping approach using piezoelectric material actuators was presented to damp out oscillation of the linkages. Zhang *et al.*[17] performed dynamic modeling and eigenvalue evaluation of a 3-RPS flexible manipulator. With combination of the substructure synthesis and FEM, an analytical approach was proposed to formulate the governing equations of motion using compatibility conditions at the interface between the limbs and the platform. Based on a sensitivity analysis, they concluded that the dimensional parameters of the 3-RPS manipulator have a slight effect on system lower natural frequencies while the joint compliances affect the distributions of lower natural frequencies significantly. The work presented by Liu *et al.*[18] concerned the dynamic modeling and solution of a 3-RRS spatial parallel manipulator with flexible links. For this purpose, they proposed a new model of spatial flexible beam elements in their FEM analysis, and derived the dynamic equations of motion using the Lagrange multiplier method.

The above review reveals that the majority of the publications, which deal with the dynamic modeling of parallel flexible manipulators, were devoted to the manipulators with 3-PRR and 3-PRS structures. To the best of our knowledge, the parallel flexible manipulators with 3-RPR structure have not been considered for dynamic analysis. Only limited studies include kinematic analysis of this type of manipulators. The kinematic study of a 3-RPR planar parallel robot whose moving platform

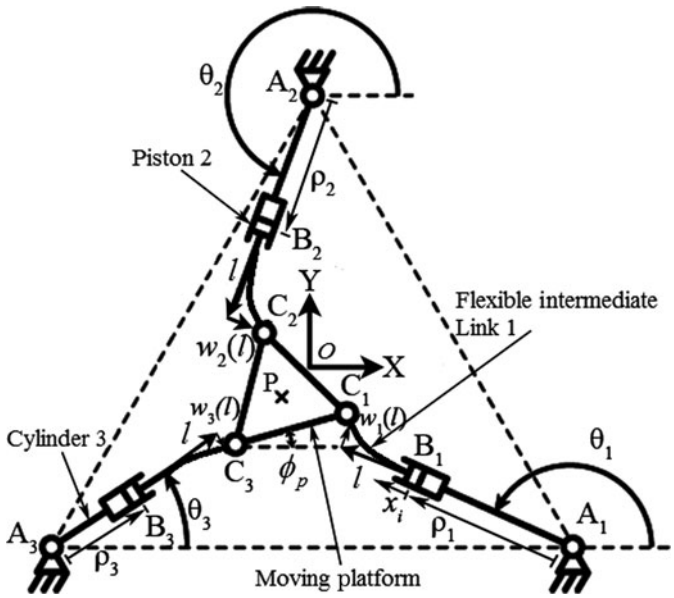

Fig. 1. Coordinates system of the proposed 3-RPR manipulator.

is connected to a fixed base by three links was presented in refs. [19] and [20]. The authors in ref. [21] described the design, construction, and control of a planar 3-RPR parallel manipulator by including forward pose kinematics but did not concern dynamic modeling strategy. Bonev *et al.*[22] described several types of singular configurations by studying the direct kinematics model of a 3-RPR planar parallel robot with actuated base joints. Recursive matrix relations for the kinematic analysis of this robot with pneumatic or hydraulic actuators were established in ref. [23]. In another study,[24] the kinematic geometry of the general 3-RPR planar parallel robots with actuated base joints was studied.

In this paper, the dynamic modeling of a 3-RPR planar parallel manipulator considering structural flexibility of its three intermediate links is studied. For flexibility modeling and derivation of equations of motion, the same procedure as used in refs. [6] and [13] for 3-PRR parallel manipulator is adopted here for the 3-RPR manipulator. These two types of manipulators are different in joint positions and in components.

The rest of the paper is as follows. The necessary steps for introducing link flexibilities and boundary conditions, imposing kinematic constraints, deriving equations of motion and solution strategies are explained. The final results will provide a new and valuable insight to the effect of different boundary conditions and link flexibility for design and control of the parallel manipulators with flexible intermediate links.

2. Coordinates System of the 3-RPR Parallel Manipulator

The planar parallel manipulator presented in this work is categorized as a 3-RPR type, as shown in Fig. 1. This manipulator, which is placed on the ground plane, is composed of three symmetric closed-loop chains, each of which consists of a revolute joint (R), then a prismatic joint (P), and again a revolute joint (R), respectively.

The moving platform consists of an equilateral triangle $C_1C_2C_3$ with three revolute joints. Note that in this manipulator both the moving platform $C_1C_2C_3$ and the fixed platform $A_1A_2A_3$ are equilateral triangles. Gravity is perpendicular to the X–Y plane of the manipulator. The end-effector is installed in the center of the moving platform. Each prismatic joint at point B_i ($i = 1, 2, 3$) is connected to the platform through a flexible link with length l. As can be perceived from the figure, two sets of local coordinates are defined for each flexible link. Coordinate x_i is assumed to be in the direction of the undeformed link i, and coordinate $w_i(x)$ is defined as the bending deflection of link i from its rigid configuration. The positive direction of $w_i(x)$ is chosen in the same direction of its corresponding θ_i. For example, $w_1(l)$ and $w_3(l)$ are shown in their negative directions, while $w_2(l)$ is shown in its positive direction. The origin O of the fixed coordinate frame is located at the center point of the

https://doi.org/10.1017/S0263574714001118 Published online by Cambridge University Press

triangle $A_1A_2A_3$. The rotation angle of each rigid link A_iB_i is specified with θ_i. The variable distance due to the actuation of prismatic joint between points B_i and A_i is defined as ρ_i.

3. Structural Flexibility Modeling of the Intermediate Links

The structural flexibility of the intermediate links is introduced based on the Euler–Bernoulli beam model and the AMM. The flexible links of this manipulator satisfy the necessary conditions for which the Euler–Bernoulli beam model can be considered. Therefore, the deflections are assumed to be small compared to the beam cross section.[25] Study on the flexibility of the joints is not discussed in this work and therefore, they are assumed rigid. Also, the platform $C_1C_2C_3$ and links A_iB_i are assumed rigid, because they are designed and built to be much stiffer than the intermediate links B_iC_i. Based on the AMM, the transverse deflections of links are modeled by an infinite number of separable harmonic modes. Since only the first few modes dominate the dynamics, the modes are truncated to a finite number of modal series. According to the formulation of the AMM, bending deformation of the flexible link i can be expressed as

$$w_i(x,t) = \sum_{j=1}^{r} \eta_{ij}(t)\psi_j(x), \quad i = 1,\ 2,\ 3, \tag{1}$$

where $w_i(x,t)$ is the bending deflection of beam that varies along the beam with time. $\psi_j(x)$ is the mode shape function and $\eta_{ij}(t)$ is the time-varying mode amplitude. Index i is the link number, j is the mode shape number, and r is the number of selected assumed modes for modeling of link flexibility. Vector of generalized flexible coordinates $\bar{\boldsymbol{\eta}}$ with dimension $3r \times 1$ is defined as

$$\bar{\boldsymbol{\eta}} = [\eta_{11}, \ldots, \eta_{1r}, \eta_{21}, \ldots, \eta_{2r}, \eta_{31}, \ldots, \eta_{3r}]^T, \tag{2}$$

where η_{ij} with $i = 1, 2, 3$ and $j = 1, \ldots, r$ denote the jth mode coordinate of the ith flexible link. The flexible intermediate links are treated as rigid in the longitudinal direction since the axial stiffness of intermediate links is much higher than the lateral stiffness. We consider both types of the fixed-pinned and fixed-free boundary conditions at each time. Due to the rigidity of the prismatic joints, the slope and deflection of the flexible links at point B_i are zero. The boundary condition at the end point C_i of the flexible links is chosen differently to investigate its effects on the vibration of the end-effector. For the fixed-pinned boundary conditions, the mode shape function $\psi_j(\xi)$ that is presented in ref. [25] can be easily developed in dimensionless form as

$$\psi_j(\xi) = \left[\left(\cos\alpha_j\xi - \cosh\alpha_j\xi\right) - \frac{\cos\alpha_j - \cosh\alpha_j}{\sin\alpha_j - \sinh\alpha_j}\left(\sin\alpha_j\xi - \sinh\alpha_j\xi\right)\right], \quad j = 1, 2, \ldots, r. \tag{3}$$

Here, $\xi = \frac{x}{l}, 0 \le \xi \le 1$, where x is the distance from B_i to an arbitrary point on the ith flexible link, and l is the link length. The parameter α_i can be obtained by solving the following frequency equation:

$$\tan\alpha_i = \tanh\alpha_i, \tag{4}$$

which can be written as $\alpha_j \approx (j + 0.25)\pi$.

On the other, for the fixed-free boundary conditions, the mode shape function $\psi_j(\xi)$ is written from ref. [25] as

$$\psi_j(\xi) = \left[\left(\cos\alpha_j\xi - \cosh\alpha_j\xi\right) - \frac{\cos\alpha_j + \cosh\alpha_j}{\sin\alpha_j + \sinh\alpha_j}\left(\sin\alpha_j\xi - \sinh\alpha_j\xi\right)\right]. \tag{5}$$

For this case, α_j is obtained from the solution of the following frequency equation:

$$\cos\alpha_j \cosh\alpha_j + 1 = 0, \tag{6}$$

https://doi.org/10.1017/S0263574714001118 Published online by Cambridge University Press

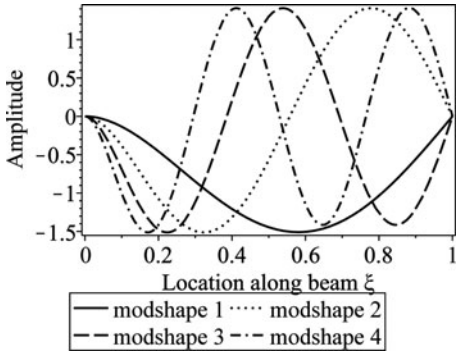

Fig. 2. Amplitude of the first four mode shapes for fixed-pinned boundary conditions.

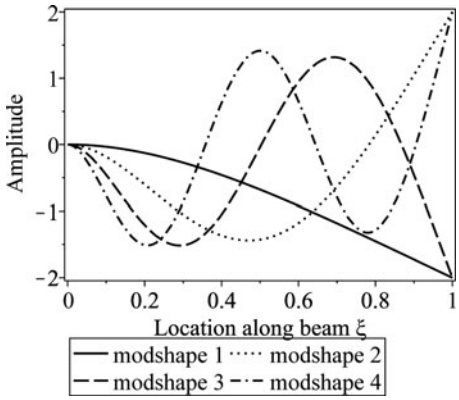

Fig. 3. Amplitude of first four mode shapes for fixed-free boundary conditions.

where, for example, α_1 to α_4 are

$$\alpha_1 = 1.875104069, \quad \alpha_2 = 4.694091133, \quad \alpha_3 = 7.854757438, \quad \alpha_4 = 10.99554073. \tag{7}$$

Figures 2 and 3 show the first four mode shapes of the flexible link for both fixed-pinned and fixed-free boundary conditions, respectively.

4. Equations of Motion of the 3-RPR Parallel Manipulator

In this section, the fully coupled equations of motion of the 3-RPR flexible parallel manipulator using Lagrange multipliers method are presented. The fixed-pinned and fixed-free boundary conditions are considered for the flexible intermediate links. For deriving the equations, the rigid body and elastic motions are incorporated as a set of generalized coordinates using the procedure outlined in refs. [13] and [14].

4.1. Kinetic energy

The total kinetic energy of the manipulator includes the kinetic energies of the cylinders (rigid links), the flexible intermediate links, and the moving platform. The kinetic energy of three rigid links A_iB_i is given as

$$T_C = \sum_{i=1}^{3} \frac{1}{2} I_c \dot{\theta}_i^2 , \tag{8}$$

https://doi.org/10.1017/S0263574714001118 Published online by Cambridge University Press

where I_c is the mass moment of inertia of the ith rigid link about its rotating axis at point A_i, and $\dot{\theta}_i$ is the angular velocity of this link. The kinetic energy of the flexible intermediate links is expressed as

$$T_L = \sum_{i=1}^{3} \frac{1}{2} \int_0^l \rho_A \left[\dot{\rho}_i^2 + ((x + \rho_i)\dot{\theta}_i + \dot{w}_i(x))^2\right] dx, \tag{9}$$

where ρ_A is mass per unit length of each flexible link with mass m,$\dot{w}_i(x)$ is the time derivative of bending deformation, and $\dot{\rho}_i$ is the linear velocity of flexible link i in the direction of its undeformed configuration. Finally, the kinetic energy of the platform is expressed as

$$T_P = \frac{1}{2} m_p \left(\dot{x}_p^2 + \dot{y}_p^2\right) + \frac{1}{2} I_p \dot{\phi}_p^2, \tag{10}$$

where I_P is the mass moment of inertia of the platform around the center point P, m_p is the platform mass, $\dot{x}_p$ and $\dot{y}_p$ are the linear velocities along the X and Y axes, respectively, and $\dot{\phi}_p$ is the angular velocity of the platform. The total kinetic energy can be obtained by summing the kinetic energy of all components as

$$T = \sum_{i=1}^{3} \frac{1}{2} I_c \dot{\theta}_i^2 + \sum_{i=1}^{3} \frac{1}{2} \int_0^l \rho_A \left[\dot{\rho}_i^2 + ((x + \rho_i)\dot{\theta}_i + \dot{w}_i(x))^2\right] dx + \frac{1}{2} m_p (\dot{x}_p^2 + \dot{y}_p^2) + \frac{1}{2} I_p \dot{\phi}_p^2. \tag{11}$$

4.2. Potential energy

The potential energy of the flexible manipulator system arises generally from two sources: the elastic deformation of flexible links and gravity. Gravitational force is perpendicular to the manipulator plane and therefore, the potential energy due to gravity is not included here. The potential energy of the system due to the bending deflection of flexible links is given as

$$V = \frac{1}{2} \sum_{i=1}^{3} \int_0^l EI \left(\frac{\partial^2 w_i(x)}{\partial x^2} \right)^2 dx = \frac{1}{2} \sum_{i=1}^{3} \frac{EI}{l^3} \int_0^1 \sum_{j=1}^{r} \eta_{ij}^2(t) (\psi_j''(\xi))^2 d\xi \,, \tag{12}$$

where E and I are the elastic modulus and the second moment of area of each flexible link, respectively.

4.3. Lagrange equations

The generalized coordinates of the manipulator include rigid and flexible coordinates. Rigid body motion is expressed by $\bar{\boldsymbol{\rho}} = [\rho_1, \rho_2, \rho_3]^T$,$\bar{\boldsymbol{\theta}} = [\theta_1, \theta_2, \theta_3]^T$, and $\bar{\mathbf{X}}_p = [X_p,\ Y_p, \phi_p]^T$. Therefore, the set of generalized coordinates is written as $\mathbf{X} = [\bar{\boldsymbol{\rho}}, \bar{\boldsymbol{\theta}}, \bar{\mathbf{X}}_\mathbf{p}, \bar{\boldsymbol{\eta}}]^T \in R^{(9+3r)\times 1}$. Three sets of rigid body coordinates are dependent due to the kinematic constraints. Since the manipulator has 3 DOFs regarding rigid body motions (without considering flexibilities), the components of $\bar{\boldsymbol{\rho}}$, $\bar{\boldsymbol{\theta}}$, and $\bar{\mathbf{X}}_P$ must satisfy six constraint equations. From the geometry of three closed-loop chains as shown in Fig. 1, following constraint equations can be written:

$$\mathbf{r}_{\mathrm{OA}_i} + \mathbf{r}_{\mathrm{A}_i\mathrm{B}_i} + \mathbf{r}_{\mathrm{B}_i\mathrm{C}_i} = \mathbf{r}_{\mathrm{OP}} + \mathbf{r}_{\mathrm{PC}_i}, \quad i = 1, 2, 3, \tag{13}$$

which upon projection along X and Y axes, six constraint equations are obtained. For the case of fixed-pinned boundary conditions, the constraint equations are expanded as

$$\Gamma_{2i-1} \equiv X_{Ai} + (\rho_i + l)\cos\theta_i - X_p - r_{PC_i}\cos(\phi_i + \phi_p) = 0, \quad i = 1, 2, 3, \tag{14}$$

$$\Gamma_{2i} \equiv Y_{Ai} + (\rho_i + l)\sin\theta_i - Y_p - r_{PC_i}\sin(\phi_i + \phi_p) = 0\,, \quad i = 1, 2, 3, \tag{15}$$

where $r_{PC_i}\cos(\varphi_i + \varphi_p)$ and $r\sin(\varphi_i + \varphi_p) = y_{ci}^0$ specify the global X and Y coordinates of C_i relative to point P (Fig. 4), respectively. Furthermore, ϕ_i is the angle between r_{PC_i} and x-axis of

https://doi.org/10.1017/S0263574714001118 Published online by Cambridge University Press

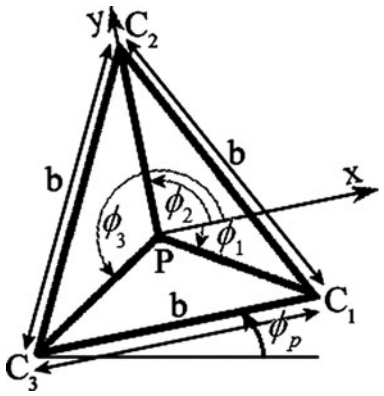

Fig. 4. Coordinate system of the moving platform.

local coordinate which according to Fig. 4, can be written as $\phi_1 = -\pi/6$, $\phi_2 = \pi/2$, and $\phi_3 = 7\pi/6$. Parameters X_{Ai} and Y_{Ai} are the global X and Y coordinates of A_i in Fig. 1, respectively. Note that the variables r_{PC_i}, ϕ_i, X_{Ai}, and Y_{Ai} are constant.

In general, the constraint equations involve elastic deformations. However, for the fixed-pinned boundary conditions, the distance B_iC_i is constant. Therefore, constraints (14) and (15) do not include the elastic coordinates. For the fixed-free boundary conditions, the corresponding constraint equations in the expanded form are written as

$$\Gamma_{2i-1} \equiv X_{Ai} + (\rho_i + l)\cos\theta_i - w_i(l)\sin\theta_i - X_p - r_{PC_i}\cos(\phi_i + \phi_p) = 0, \quad i = 1, 2, 3, \tag{16}$$

$$\Gamma_{2i} \equiv Y_{Ai} + (\rho_i + l)\sin\theta_i + w_i(l)\cos\theta_i - Y_p - r_{PC_i}\sin(\phi_i + \phi_p) = 0, \quad i = 1, 2, 3. \tag{17}$$

Using the Lagrange multiplier method, the dynamic equations of the manipulator are given as

$$\frac{\mathrm{d}}{\mathrm{d}t}\left(\frac{\partial(T-V)}{\partial \dot{X}_j}\right) - \frac{\partial(T-V)}{\partial X_j} = Q_j + \sum_{k=1}^{6}\lambda_k \frac{\partial \Gamma_k}{\partial X_j}, \quad j = 1, \ldots, (9+3r), \tag{18}$$

where Q_j is the generalized force associated with the generalized coordinate X_i, and λ_k is the Lagrange multiplier associated with the kth constraint equation. Substituting the relations of kinetic and potential energies together with constraint equations in Eq. (18) results the manipulator differential-algebraic equations which can be rearranged in the following matrix form as

$$\begin{bmatrix} \mathbf{M}_{\rho\rho} & \mathbf{0} & \mathbf{0} & \mathbf{0} \\ \mathbf{0} & \mathbf{M}_{\theta\theta} & \mathbf{0} & \mathbf{M}_{\eta\theta}^T \\ \mathbf{0} & \mathbf{0} & \mathbf{M}_{X_P X_P} & \mathbf{0} \\ \mathbf{0} & \mathbf{M}_{\eta\theta} & \mathbf{0} & \mathbf{M}_{\eta\eta} \end{bmatrix} \begin{bmatrix} \ddot{\bar{\boldsymbol{\rho}}} \\ \ddot{\bar{\boldsymbol{\theta}}} \\ \ddot{\bar{\boldsymbol{X}}}_{\mathrm{P}} \\ \ddot{\bar{\boldsymbol{\eta}}} \end{bmatrix} + \begin{bmatrix} \mathbf{K}_{\rho\rho} & \mathbf{0} & \mathbf{0} & \mathbf{0} \\ \mathbf{K}_{\theta\rho} & \mathbf{0} & \mathbf{0} & \mathbf{0} \\ \mathbf{0} & \mathbf{0} & \mathbf{0} & \mathbf{0} \\ \mathbf{0} & \mathbf{0} & \mathbf{0} & \mathbf{K}_{\eta\eta} \end{bmatrix} \begin{bmatrix} \bar{\boldsymbol{\rho}} \\ \bar{\boldsymbol{\theta}} \\ \bar{\boldsymbol{X}}_{\mathrm{P}} \\ \bar{\boldsymbol{\eta}} \end{bmatrix} = \begin{bmatrix} \mathbf{F}_{c\rho} \\ \mathbf{F}_{c\theta} \\ \mathbf{0} \\ \mathbf{F}_{c\eta} \end{bmatrix}$$

$$+ \begin{bmatrix} \mathbf{F}_{e\rho} \\ \mathbf{F}_{e\theta} \\ \mathbf{F}_{eX_P} \\ \mathbf{F}_{e\eta} \end{bmatrix} + \begin{bmatrix} \mathbf{J}_{\Gamma\rho}^T \\ \mathbf{J}_{\Gamma\theta}^T \\ \mathbf{J}_{\Gamma X_P}^T \\ \mathbf{J}_{\Gamma\eta}^T \end{bmatrix} \begin{bmatrix} \lambda_1 \\ \lambda_2 \\ \lambda_3 \\ \lambda_4 \\ \lambda_5 \\ \lambda_6 \end{bmatrix}, \tag{19}$$

where vectors $\mathbf{F}_{ci}$, $(i = \rho, \theta, X_P, \eta)$, include Coriolis and centrifugal forces, vectors $\mathbf{F}_{ei}$ contain externally applied forces, and $\mathbf{J}_{\Gamma i}$ are the constraint Jacobian matrices corresponding to the generalized coordinates. Matrices $\mathbf{M}$ and $\mathbf{K}$ are the mass and stiffness matrices, respectively. The detailed derivation of the above parameters is given in the Appendix. It is maybe important to notice that some of the parameters appeared in Eq. (19) are different for two types of the already considered

https://doi.org/10.1017/S0263574714001118 Published online by Cambridge University Press

Table I. Planar 3-RPR manipulator's parameters.

Moving platform	Side length ($C_iC_{i+1} = b$)	100 mm
	Mass	0.2 kg
Flexible links	Length ($B_iC_i = l$)	200 mm
	Cross section diameter	10 mm
	Density	2270kg/m^3
	Young's modulus	73 GPa
Cylinders (rigid links)	Motion course amplitude (A_iB_i)	200 mm
	Inner diameter	14 mm
	Outer diameter	16 mm
	Density	2270kg/m^3
Fixed platform	Side length (A_iA_{i+1})	660 mm

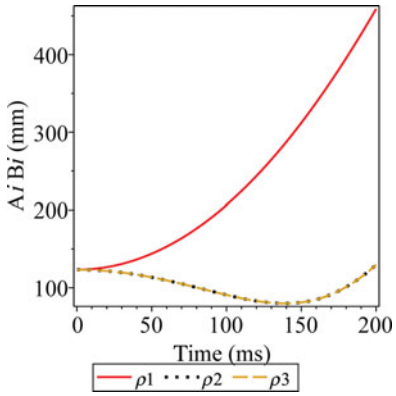

Fig. 5. Variations of $\rho_i(t)$for $\mathbf{F}_{e\rho} = [5, 0, 0]^T$.

boundary conditions. The dimension of Eq. (19) is $(9 + 3r) \times (9 + 3r)$ where r is number of the assumed modes.

5. Numerical Simulation

In this section, some numerical simulations for the 3-RPR parallel manipulator with three flexible intermediate links are presented. In these simulations, the first three mode shapes are selected to model the structural flexibility of the intermediate links, i.e., $r = 3$. Consequently, Eq. (19) would consist of 18 equations in terms of 24 unknowns, which should be considered together with six constraint equations. Table I reports the necessary parameters of the manipulator.

The initial conditions for all simulations are considered to be zero. The center of moving platform at the beginning is coinciding with the origin O of the fixed frame. For this configuration, the initial generalized coordinates $\bar{\boldsymbol{\rho}}_0$ and $\bar{\boldsymbol{\theta}}_0$ can be calculated from the constraint equations based on an inverse kinematics approach as

$$\bar{\boldsymbol{\rho}}_0 = \left(560\frac{\sqrt{3}}{3} - 200\right)\begin{bmatrix}1 & 1 & 1\end{bmatrix}^T, \quad \bar{\boldsymbol{\theta}}_0 = \frac{\pi}{6}\begin{bmatrix}5 & 9 & 1\end{bmatrix}^T. \tag{20}$$

In the following, three different simulations are carried out to validate the equations of motion. Additionally, the effect of considering each type of boundary conditions is investigated. The approach that is used for numerical solving of Eq. (19) is the Modified Extended Backward-Differentiation Formula Implicit (MEBDFI) of the Maple software.

Simulation 1: A constant external force

In this example, only a constant external force of 5 N corresponding to the generalized coordinate ρ_1 is applied to the manipulator with fixed-pinned boundary conditions by the piston at B_1, while

https://doi.org/10.1017/S0263574714001118 Published online by Cambridge University Press

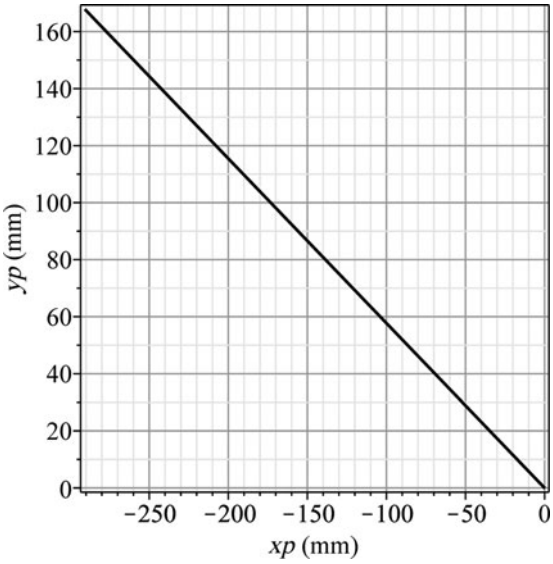

Fig. 6. End-effector trajectory for $\mathbf{F}_{e\rho} = [5, 0, 0]^T$.

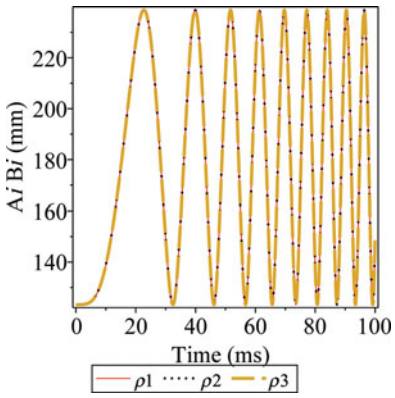

Fig. 7. Variations of $\rho_i(t)$, for $\mathbf{F}_{eXp} = [0, 0, 5]^T$.

other generalized forces are kept zero. Figures 5 and 6 display the variations of $\rho_i(t)$, $(i = 1, 2, 3)$, with respect to time and the end-effector trajectory, respectively. According to the applied force and manipulator geometry, parameter ρ_1 is increased, while ρ_2 and ρ_3 are reduced with the same rate. This result can also be realized by direct inspection of the manipulator due to the symmetry. The coordinates ρ_2 and ρ_3 begin to increase when side C_2C_3 of the moving platform reaches to side A_2A_3 of the fixed platform. In Fig. 6, the end-effector trajectory is on a straight line in the direction of the applied force with an angle of 30° with respect to side A_2A_3. These results verify the overall behavior of the manipulator in a simple simulation.

Simulation 2: A constant external torque

In the second example, only a constant torque of 5 Nm is applied to the moving platform of the manipulator with fixed-pinned boundary conditions while other generalized forces are kept zero. The torque rotates the platform around its center and consequently, the pistons at points B_i follow a reciprocal motion along the cylinders A_iB_i, as shown in Fig. 7. Variation of the rotation angle of three cylinders A_iB_i is illustrated in Fig. 8. The pistons reciprocal velocity and the angular velocity of three cylinders are increasing, due to the result of applied torque. This important fact can simply be realized from Figs. 7 and 8.

https://doi.org/10.1017/S0263574714001118 Published online by Cambridge University Press

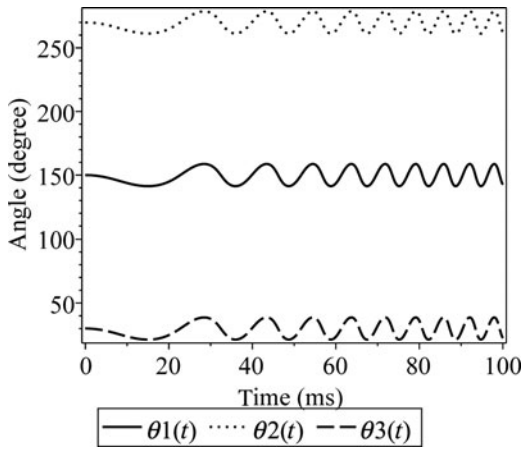

Fig. 8. Variations of $\theta_i(t)$ for $\mathbf{F}_{eXp} = [0, 0, 5]^T$.

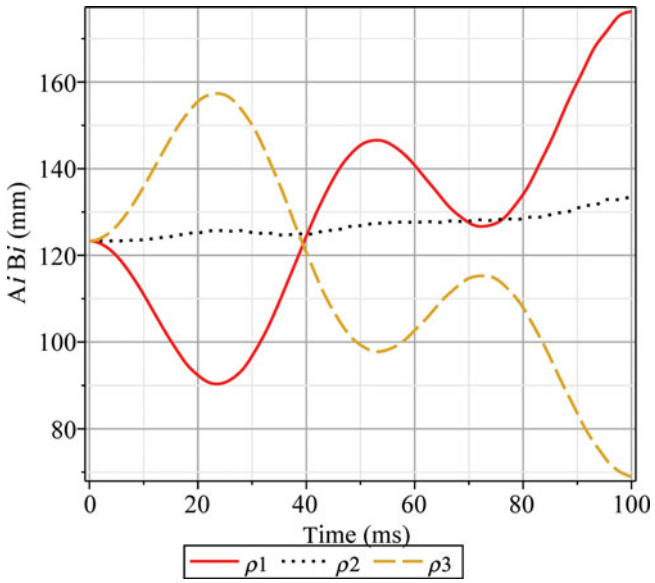

Fig. 9. Variations of $\rho_i(t)$ for the case of harmonic forces.

Simulation 3: Harmonic forces

In this section, some typical harmonic forces are applied to the manipulator with both types of fixed-pinned and fixed-free boundary conditions. The harmonic forces are considered as

$$\mathbf{F}_{e\rho} = (50\cos(40\pi\, t) - 50)\,[1 \;\; 1 \;\; 1]^T \text{ (N)}, \quad \mathbf{F}_{e\theta} = 5\cos(400\pi\, t)\,[1, 1, 1]^T \text{ (Nm)}$$
$$\mathbf{F}_{eXp} = [100\cos(40\pi\, t)(\text{N}), 0, 0]^T, \quad \mathbf{F}_{e\eta} = \mathbf{0}_{9\times 1}.$$

These external forces have been selected in such a way that the structural flexibility of the intermediate links would be excited. For this purpose, the system of Eqs. (19) is first generated for two types of boundary conditions, and then, is solved using the MEBDFI approach. The fixed-pinned boundary conditions are used for illustrating the rigid body motion. On other hand, the fixed-free boundary conditions are used for investigating the effect of link flexibility on the end-effector trajectory. The results are depicted in Figs. 9–11. In this paper, we have not imposed any constraint to restrict the increase of the cylinders length from their maximum length. This important fact has been remedied by proper selection of applied forces.

Figure 9 illustrates the variation of three coordinates, ρ_i(i = 1, 2, 3). It is observed that for two types of boundary conditions, variations of $\rho_i$coincide with each other. This fact is the direct result of

https://doi.org/10.1017/S0263574714001118 Published online by Cambridge University Press

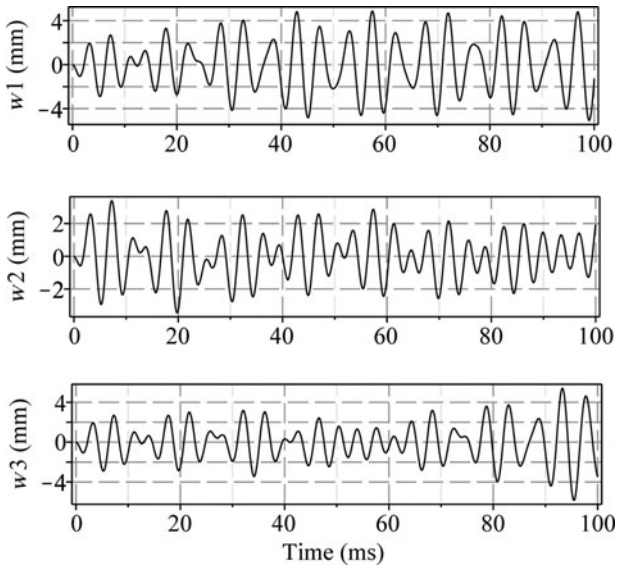

Fig. 10. Bending deformation of point C_i $(i = 1,\ 2,\ 3)$ for the case of fixed-free boundary conditions.

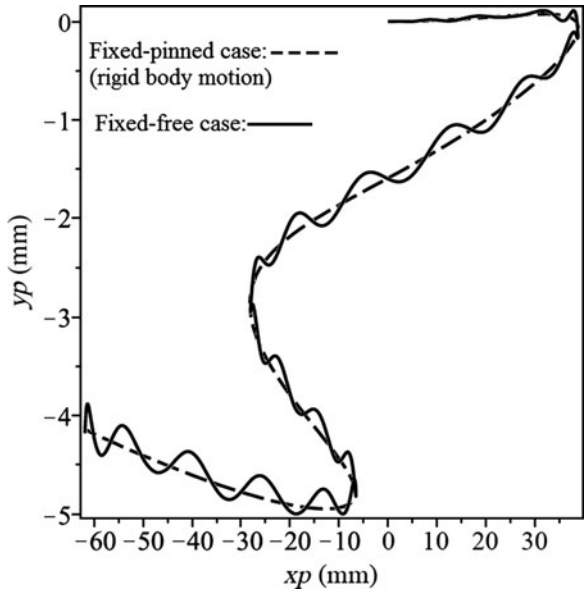

Fig. 11. The trajectory of the end-effector for both types of the boundary conditions.

neglecting longitudinal flexibility of the flexible links. Figure 10 shows the bending deformations of the flexible links tip at C_i for the fixed-free boundary conditions. Vibrations of C_i for the fixed-pinned conditions would not be significant and therefore, have not been considered here.

Figure 11 compares the end-effector trajectory for both types of the boundary conditions. For this case, the global X and Y coordinates of point P on the end-effector are obtained from simulation of the manipulator with both boundary conditions. As can clearly be seen, when the fixed-pinned boundary conditions are assumed, flexibility of the intermediate links does not affect the trajectory significantly. This means that the trajectory is almost close to the case of rigid manipulator. However, for the fixed-free boundary conditions, the end-effector experiences significant periodic vibrations during passing through the trajectory. This important issue is due to the effect of imposing different boundary conditions at points C_i(i = 1, 2, 3) on the vibrations of the platform. It means that considering the fixed-pinned boundary conditions would not show any considerable effect of the structural bending flexibilities on the end-effector vibration. In this case, the flexible manipulator behaves almost rigid.

https://doi.org/10.1017/S0263574714001118 Published online by Cambridge University Press

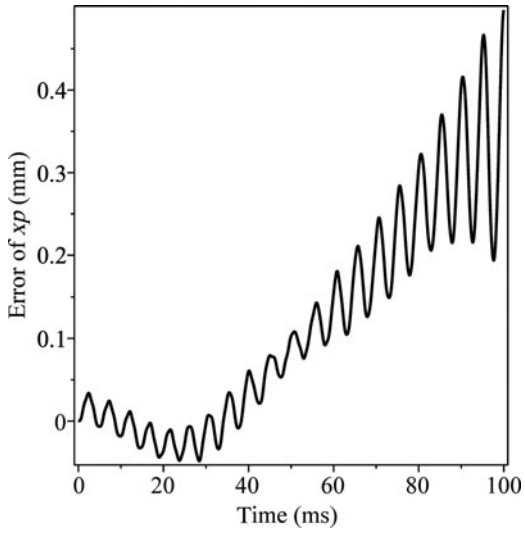

Fig. 12. Error of X position.

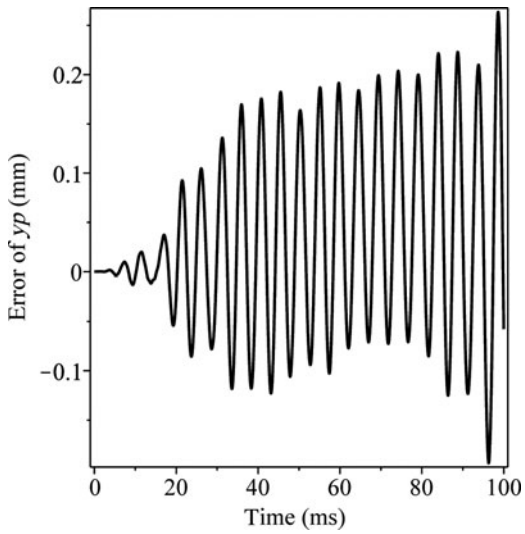

Fig. 13. Error of Y position.

On the other hand, the fixed-free boundary conditions transfer correctly the induced vibrations of the flexible links to the moving platform.

For investigating more exactly the effects of two boundary conditions on the end-effector trajectory, the difference between the trajectories of Fig. 11 are obtained for the global $X$and Y coordinates, separately. Figures 12 and 13 show these two cases with respect to time, respectively.

It can clearly be seen that for both coordinates, the difference grows gradually with an oscillating behavior. This issue can affect the required level of precision when modeling a flexible manipulator. In addition, to assess further the effect of considering different boundary conditions, Figs. 14 and 15 illustrate the velocity of the end-effector in the $X$and Y directions, respectively. Also, Fig. 16 shows the angular position of the end-effector with respect to time. For all plots, the fixed-free boundary conditions impose higher oscillation of the manipulator end-effector.

6. Conclusion

In this paper, the equations of motion of a planar parallel manipulator 3-RPR with three flexible intermediate links were derived. The intermediate links are modeled as Euler–Bernoulli beams with

https://doi.org/10.1017/S0263574714001118 Published online by Cambridge University Press

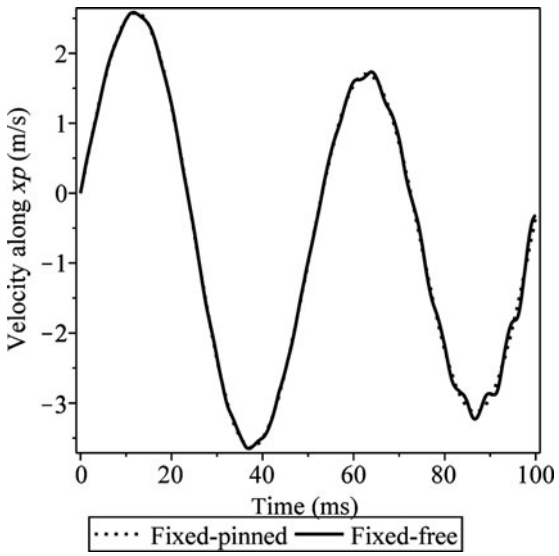

Fig. 14. Velocity along the X-axis for the end-effector.

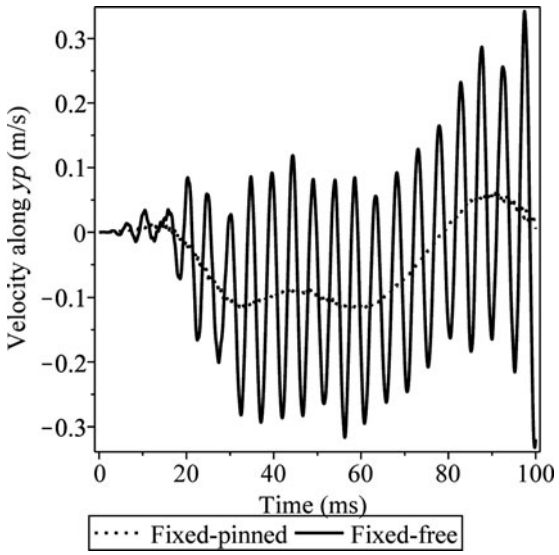

Fig. 15. Velocity along the Y-axis for the end-effector.

the fixed-pinned and the fixed-free boundary conditions based on the AMM. The equations of motion of the 3-RPR manipulator are formulated using the augmented Lagrange multipliers method in the form of differential algebraic equations (DAEs) by incorporating the elastic and rigid coordinates in the set of generalized coordinates. Six kinematic constraints were defined to establish the necessary relations between generalized coordinates. Three different simulations were performed. In the first and the second simulations, a constant external force and a constant external torque was applied, respectively. The fixed-pinned boundary conditions were considered for this case. The results verified the overall dynamic response of the manipulator. In the last simulation, some typical harmonic forces were applied to the manipulator with both types of the fixed-pinned and fixed-free boundary conditions. It was realized that considering the fixed-pinned boundary conditions would not show any considerable effect of structural bending flexibilities on the end-effector vibration. In this case, the flexible manipulator behaves almost rigid. On the other hand, the fixed-free boundary conditions transfer correctly the induced vibrations of the flexible links to the moving platform, which in turn

https://doi.org/10.1017/S0263574714001118 Published online by Cambridge University Press

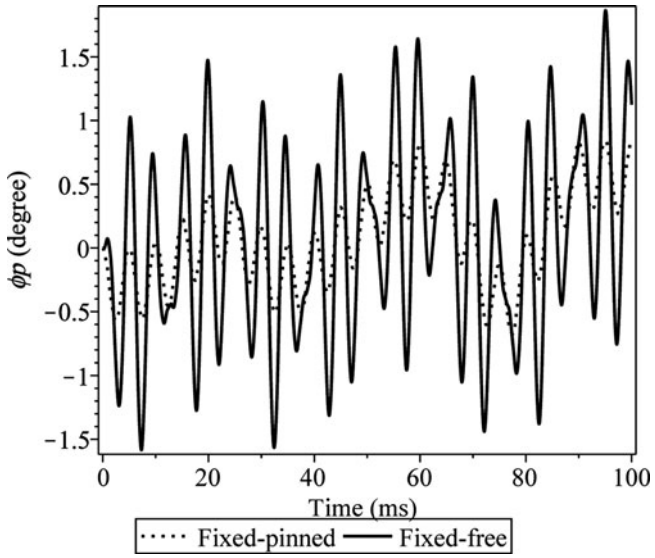

Fig. 16. Angular position of the end-effector.

caused the end-effector to experience significant periodic vibrations during passing through the trajectory.

Appendix

Mass matrix:

$$\mathbf{M}_{\rho\rho} = m\begin{bmatrix}1&0&0\\0&1&0\\0&0&1\end{bmatrix}, \mathbf{M}_{\theta\theta} = \left(I_c + \frac{ml^2}{3}\right)\begin{bmatrix}1&0&0\\0&1&0\\0&0&1\end{bmatrix} + m\begin{bmatrix}l\rho_1+\rho_1^2&0&0\\0&l\rho_2+\rho_2^2&0\\0&0&l\rho_3+\rho_3^2\end{bmatrix},$$

$$\mathbf{M}_{X_PX_P} = \begin{bmatrix}m_p&0&0\\0&m_p&0\\0&0&I_p\end{bmatrix}, \mathbf{M}\eta\eta = m\begin{bmatrix}\hat{\mathbf{M}}&0&0\\0&\hat{\mathbf{M}}&0\\0&0&\hat{\mathbf{M}}\end{bmatrix} \in R^{3r\times 3r},$$

$$\hat{\mathbf{M}} = \begin{bmatrix}\int_0^1 \psi_1^2 d\xi & \cdots & 0\\ \vdots & \ddots & \vdots\\ 0 & \cdots & \int_0^1 \psi_r^2 d\xi\end{bmatrix} \in R^{r\times r},$$

$$\mathbf{M}_{\eta\theta} = ml\begin{bmatrix}M_{11}&0&0\\ \vdots&\vdots&\vdots\\ M_{r1}&0&0\\ 0&M_{12}&0\\ \vdots&\vdots&\vdots\\ 0&M_{r2}&0\\ 0&0&M_{13}\\ \vdots&\vdots&\vdots\\ 0&0&M_{r3}\end{bmatrix}, M_{ij} = \int_0^1 \psi_i \xi d\xi + \frac{\rho_j \int_0^1 \psi_i d\xi}{l}.$$

https://doi.org/10.1017/S0263574714001118 Published online by Cambridge University Press

Stiffness matrix:

$$\mathbf{K}_{\rho\rho} = -m\begin{bmatrix} \dot{\theta}_1^2 & 0 & 0 \\ 0 & \dot{\theta}_2^2 & 0 \\ 0 & 0 & \dot{\theta}_3^2 \end{bmatrix}, \mathbf{K}_{\theta\rho} = 2m\begin{bmatrix} \dot{\rho}_1\dot{\theta}_1 & 0 & 0 \\ 0 & \dot{\rho}_2\dot{\theta}_2 & 0 \\ 0 & 0 & \dot{\rho}_3\dot{\theta}_3 \end{bmatrix}, \mathbf{K}_{\eta\eta} = \frac{EI}{l^3}\begin{bmatrix} \hat{\mathbf{K}} & \mathbf{0} & \mathbf{0} \\ \mathbf{0} & \hat{\mathbf{K}} & \mathbf{0} \\ \mathbf{0} & \mathbf{0} & \hat{\mathbf{K}} \end{bmatrix} \in R^{3r\times 3r},$$

$$\hat{\mathbf{K}} = \begin{bmatrix} \int_0^1 \psi_1''^2 d\xi & \cdots & 0 \\ \vdots & \ddots & \vdots \\ 0 & \cdots & \int_0^1 \psi_r''^2 d\xi \end{bmatrix} \in R^{r\times r}.$$

Coriolis and centrifugal forces:

$$\mathbf{F}_{c\rho} = \begin{bmatrix} (0.5ml)\dot{\theta}_1^2 + \sum_{j=1}^{r} m\dot{\eta}_{1j}\dot{\theta}_1 \int_0^1 \psi_j d\xi \\ (0.5ml)\dot{\theta}_2^2 + \sum_{j=1}^{r} m\dot{\eta}_{2j}\dot{\theta}_2 \int_0^1 \psi_j d\xi \\ (0.5ml)\dot{\theta}_3^2 + \sum_{j=1}^{r} m\dot{\eta}_{3j}\dot{\theta}_3 \int_0^1 \psi_j d\xi \end{bmatrix}, \quad \mathbf{F}_{c\theta} = -m\begin{bmatrix} l\dot{\rho}_1\dot{\theta}_1 + \sum_{j=1}^{r} \dot{\rho}_1\dot{\eta}_{1j} \int_0^1 \psi_j d\xi \\ l\dot{\rho}_2\dot{\theta}_2 + \sum_{j=1}^{r} \dot{\rho}_2\dot{\eta}_{2j} \int_0^1 \psi_j d\xi \\ l\dot{\rho}_3\dot{\theta}_3 + \sum_{j=1}^{r} \dot{\rho}_3\dot{\eta}_{3j} \int_0^1 \psi_j d\xi \end{bmatrix},$$

$$\mathbf{F}_{c\eta} = \begin{bmatrix} \dot{\rho}_1\dot{\theta}_1 \int_0^1 \psi_1 d\xi & \ldots & \dot{\rho}_1\dot{\theta}_1 \int_0^1 \psi_r d\xi & \dot{\rho}_2\dot{\theta}_2 \int_0^1 \psi_1 d\xi & \ldots & \dot{\rho}_2\dot{\theta}_2 \int_0^1 \psi_r d\xi & \dot{\rho}_3\dot{\theta}_3 \int_0^1 \psi_1 d\xi & \ldots & \dot{\rho}_3\dot{\theta}_3 \int_0^1 \psi_r d\xi \end{bmatrix}^T$$

Jacobian matrix:

$$\mathbf{J}_{\Gamma 1}^T = \begin{bmatrix} \cos\theta_1 & \sin\theta_1 & 0 & 0 & 0 & 0 \\ 0 & 0 & \cos\theta_2 & \sin\theta_2 & 0 & 0 \\ 0 & 0 & 0 & 0 & \cos\theta_3 & \sin\theta_3 \end{bmatrix},$$

$$\mathbf{J}_{\Gamma 2}^T = \begin{bmatrix} -s2_1 & c2_1 & 0 & 0 & 0 & 0 \\ 0 & 0 & -s2_2 & c2_2 & 0 & 0 \\ 0 & 0 & 0 & 0 & -s2_3 & c2_3 \end{bmatrix},$$

where for the fixed-pinned boundary conditions, $s2_i = (\rho_i + l)\sin\theta_i$ and $c2_i = (\rho_i + l)\cos\theta_i$. Also, for the fixed-free boundary conditions, $s2_i = (\rho_i + l)\sin\theta_i + \cos\theta_i \sum_{j=1}^{r} \eta_{ij}\psi_j(1)$ and $c2_i = (\rho_i + l)\cos\theta_i - \sin\theta_i \sum_{j=1}^{r} \eta_{ij}\psi_j(1)$.

$$\mathbf{J}_{\Gamma 3}^T = \begin{bmatrix} -1 & 0 & -1 & 0 & -1 & 0 \\ 0 & -1 & 0 & -1 & 0 & -1 \\ s3_1 & -c3_1 & s3_2 & -c3_2 & s3_3 & -c3_3 \end{bmatrix}, \quad s3_i = r\sin(\phi_i + \phi_p), c3_i = r\cos(\phi_i + \phi_p).$$

https://doi.org/10.1017/S0263574714001118 Published online by Cambridge University Press

For the fixed-pinned boundary conditions $\mathbf{J}_{\Gamma 4} = \mathbf{0}$, and for the fixed-free boundary conditions,

$$\mathbf{J}_{\Gamma 4}^{T} = \begin{bmatrix} -s4_{11} & c4_{11} & 0 & 0 & 0 & 0 \\ -s4_{12} & c4_{12} & 0 & 0 & 0 & 0 \\ -s4_{13} & c4_{13} & 0 & 0 & 0 & 0 \\ 0 & 0 & -s4_{21} & c4_{21} & 0 & 0 \\ 0 & 0 & -s4_{22} & c4_{22} & 0 & 0 \\ 0 & 0 & -s4_{23} & c4_{23} & 0 & 0 \\ 0 & 0 & 0 & 0 & -s4_{31} & c4_{31} \\ 0 & 0 & 0 & 0 & -s4_{32} & c4_{32} \\ 0 & 0 & 0 & 0 & -s4_{33} & c4_{33} \end{bmatrix}, \quad s4_{ij} = \sin\theta_i \cdot \psi_j(1), c4_{ij} = \cos\theta_i \cdot \psi_j(1).$$

References

1. S. K. Dwivedy and P. Eberhard, "Dynamic analysis of flexible manipulators, a literature review," *Mech. Mach. Theory* **41**, 749–777 (2006).
2. R. J. Theodore and A. Ghosal, "Comparison of the assumed modes and finite element models for flexible multi-link manipulators," *Int. J. Robot. Res.* **14**, 91–111 (1995).
3. J. D. Lee and Z. Geng, "A Dynamic model of a flexible Stewart platform," *Comput. Struct.* **48**, 367–374 (1993).
4. M. Giovagnoni, "Dynamics of Flexible Closed-Chain Manipulator," *ASME Design Technical Conference*, Scottsdale, Arizona, USA (Sep. 13–16, 1992) pp. 483–490.
5. A. Fattah, J. Angeles and A. K. Misra, "Dynamics of a 3-DOF Spatial Parallel Manipulator with Flexible Links," *Proceedings IEEE International Conference on Robotics and Automation*, Nagoya, Japan (May 21–27, 1995) pp. 627–632.
6. B. Kang and J. K. Mills, "Dynamic modeling of structurally-flexible planar parallel manipulator," *Robotica* **20**, 329–339 (2002).
7. X. Wang and J. K. Mills, "Experimental Modal Analysis of Flexible Linkages in a Smart Parallel Platform," *Proceeding of the 7th CANSMART Meeting – International Workshop on Smart Materials and Structures*, Montreal, Canada (Oct. 21–22, 2004) pp. 37–46.
8. G. Piras, W. L. Cleghorn, and J. K. Mills, "Dynamic finite-element analysis of a planar high speed, high-precision parallel manipulator with flexible links," *Mech. Mach. Theory* **40**, 849–862 (2005).
9. X. Wang, and J. K. Mills, "FEM dynamic model for active vibration control of flexible linkages and its application to a planar parallel manipulator," *J. Appl. Acoust.* **66**, 1151–1161 (2005).
10. Z. Zhou, J. Xi and C. K. Mechefske, "Modeling of a fully flexible 3PRS manipulator for vibration analsysis," *J. Mech. Des.* **128**, 403–412 (2006).
11. X. Zhang, J. K. Mills and W. L. Cleghorn, "Study on the Effect of Elastic Deformations on Rigid Body Motions of a 3-PRR Flexible Parallel Manipulator," *Proceedings of the 2007 IEEE International Conference on Mechatronics and Automation*, Harbin, China (Aug. 5–8, 2007) pp. 1805–1810.
12. X. Zhang, J. K. Mills and W. L. Cleghorn, "Dynamic modeling and experimental validation of a 3-PRR parallel manipulator with flexible intermediate links," *J. Intell. Robot. Syst.* **50**, 323–340 (2007).
13. X. Zhang, J. K. Mills and W. L. Cleghorn, "Coupling characteristics of rigid body motion and elastic deformation of a 3-PRR parallel manipulator with flexible links," *Multibody Syst. Dyn.* **21**, 167–192 (2009).
14. X. Zhang, J. K. Mills and W. L. Cleghorn, "Investigation of axial forces on dynamic properties of a flexible 3-PRR planar parallel manipulator moving with high speed," *Robotica* **28**, 607–619 (2010).
15. X. Zhang, J. K. Mills and W. L. Cleghorn, "Multi-Mode vibration control and position error analysis of parallel manipulator with multiple flexible links," *Trans. Can. Soc. Mech. Eng.* **34**, 197–213 (2010).
16. B. Kang and J. K. Mills, "Dynamic Modelling and Vibration Control of a Planar Parallel Manipulator with Structurally Flexible Linkages," **In**: *Parallel Manipulators, New Developments* (J. H. Ryu, ed.), (Vienna, Austria, 2008) pp. 405–426.
17. J. Zhang, Y. Li and T. Huang, "Dynamic modeling and eigenvalue evaluation of a 3-DOF PKM module," *Chinese J. Mech. Eng.* **23**, 166–173 (2010).
18. S. Z. Liu, Y. Q. Yu and Z. C. Zhu, "Dynamic modeling and analysis of 3-RRS parallel manipulator with flexible links," *J. Cent. South Univ. Technol.* **17**, 323–331 (2010).
19. C. Gosselin and J. Angeles, "The optimum kinematic design of a planar three-degree-of-freedom parallel manipulator," *ASME J. Mech. Trans. Auto. Des.* **110**, 35–41 (1988).
20. G. R. Pennock and D. J. Kassner, "Kinematic analysis of a planar eight-bar linkage: application to a platform-type robot," *J. Mech. Des.* **114**, 87–95 (1992).
21. R. L. Williams and A. R. Joshi, "Planar Parallel 3-RPR Manipulator," *Proceedings of the Sixth Conference on Applied Mechanisms and Robotics*, Cincinnati, USA (Dec. 12–15, 1999) pp. 1–8.

22. I. Bonev, D. Zlatanov and C. Gosselin, "Singularity analysis of 3-DOF planar parallel mechanisms via screw theory," *J. Mech. Des.* **25**, 573–581 (2003).
23. S. Staicu, D. C. Carp-Ciocardia and A. Codoban, "Kinematics modelling of a planar parallel robot with prismatic actuators," *U.P.B. Sci. Bull., Series D* **69**, 3–14 (2007).
24. S. Briot, I. Bonev, D. Chablat, P. Wenger and V. Arakelian, "Self-motions of general 3-RPR planar parallel robots," *Int. J. Robot. Res.* **27**, 855–866 (2008).
25. S. S. Rao, *Vibration of Continuous Systems* (Wiley, New York, 2007).

https://doi.org/10.1017/S0263574714001118 Published online by Cambridge University Press